ORIGINAL ARTICLE

Carbazole-based Schiff base: A sensitive fluorescent 'turn-on' chemosensor for recognition of Al(III) ions in aqueous-alcohol media

Feyza Kolcu [a,b], İsmet Kaya [a,*]

[a] Çanakkale Onsekiz Mart University, Faculty of Science and Arts, Department of Chemistry, Polymer Synthesis and Analysis Lab., Çanakkale, Turkey
[b] Lapseki Vocational School, Department of Chemistry and Chemical Processing Technologies, Çanakkale Onsekiz Mart University, Çanakkale, Turkey

Abstract Carbazole-based Schiff base chemosensor was synthesized in one-pot synthesis using 2-hydroxy-1-naphtaldehyde for fluorescent sensing of Al^{3+} ions. Characterization of the ligand (L) was revealed through spectroscopic and physicochemical techniques. The fluorescence emission responses of L to various metal ions and anions were investigated. The chelation was studied by UV–vis, ^1H NMR, LC-MS/MS, fluorescence titration and Job's plot analysis. Bathochromic shift resulted from charge transfer from L to electrophilic Al^{3+} ion was observed in the chelation of L with Al^{3+}. The potentiality of L to be a distinguished probe to detect Al^{3+} ions was due to a chelation enhanced fluorescence (CHEF) effect, concomitant with noticeable fluorescent enhancement. A significant fluorescence enhancement at 533 nm was observed in ethanol–water (1:1, v/v) solution upon addition of Al^{3+} along with a distinct color change from yellow to white. Non-fluorescent ligand exposed highly sensitive turn-on fluorescent sensor behavior for selectively sensing Al^{3+} ions via 1:1 (ligand:metal) stoichiometry. The ligand's specificity in the existence of other tested metal ions and anions indicated no observation in color change. The ligand-Al^{3+} complex formation was reversible upon addition of chelating agent EDTA. The ligand interacted with Al^{3+} ions with an association constant of $K_a = 5 \times 10^4 M^{-1}$. The limit of detection (LOD) was found to be 2.59×10^{-7} M. The synthesized Schiff base could efficiently detect Al^{3+} ions as a fluorescent sensor.

* Corresponding author.
E-mail address: ikaya@comu.edu.tr (İ. Kaya).

1. Introduction

Hugo Schiff discovered Schiff bases with an azomethine or imine functional group on occasion of a condensation reaction between aldehydes or ketones and amines (Schiff, 1864). Schiff bases have been discussed in a vast diversity of biological activ-

ities such as antimicrobial (Da Silva et al., 2011), anti-inflammatory (Kajal et al., 2013), antioxidant (Teran et al., 2019), anticancer (Shah et al., 2020), antitumor (Min et al., 2022), etc. The presence of –HC = N- (imine-azomethine) group are suited for binding various metal ions via lone pairs of the nitrogen atom. Schiff bases which are considered as the privileged ligands are the backbone of a large number of organic compounds in a broad area of implementations such as material science, catalysis, bioinorganic, biological, analytical and organic chemistry (Arunadevi and Raman, 2020).

Various Schiff bases have been discussed as sensors for sensing of metal ions in aqueous systems (Berhanu et al., 2019; Iacopetta et al., 2021). Schiff base ligands have been of interest to researchers in coordination chemistry providing useful pharmacological and physiological activities due to their ease of synthesis and their potentiality to form complexes with metal ions (Abu-Dief and Mohamed, 2015) and their investigation in medicinal, biophysics, light emitting diodes and industrial functionalities such as fuel additives (Bar et al., 2016), corrosion inhibitor (Singh et al. 2015), coupling catalyst (Suzuki-Miyaura) (Arumugam et al., 2015), enzyme inhibitor (Rahim et al., 2016), liquid crystal, light emitting diodes, laser technology, biophysics, selective colorimetric, optical and fluorescent sensors for ions, magnetic resonance imaging (MRI) sensor (Tiwari et al., 2013; Zhu et al., 2015) nucleic acid conjunction cleavage (Yadav et al., 2015) and antitubercular agent (Jamadar et al., 2012).

The researchers of biological, chemical and environmental sciences have immense importance to detection of metal ions, small anions and biomolecules (Chang et al., 2015; Jiang et al., 2020; Wu et al., 2017). Recently, the development of chemosensors has demonstrated a great research subject as they possess superiorities in terms of easiness in operation, good selectivity and high sensitivity (Roy, 2021; Roy et al., 2021; Yin et al., 2021). Of particular interest is the design of selective "turn-on" fluorescent sensors in consequence of fluorescence emission enhancement (Hirayama et al., 2013; Jun et al., 2011; Kolcu et al., 2021; Yu et al., 2017; Yu and Wu, 2014). Schiff bases have been of important among the prominent chemosensors for selective sensing of metal ions (Jakubek et al., 2017; Udhayakumari and Inbaraj, 2020; Kolcu et al., 2020; Fan et al., 2020; He et al., 2021). The predominant decay stage of the excited state is the C = N isomerization of the compounds, which are often nonfluorescent (Yan et al., 2016; Tang et al., 2011; Wu et al., 2007).

The detection of Al^{3+}, which is the third most abundant element after oxygen and silicon in the earth' crust (Burgess, 1996; Soni et al., 2001), is of great interest due to its common implementation in human activities such as in production of computers, automobiles, electrical equipments, packaging materials, cooking utensils, foods and food ingredients, clinical drugs such as buffered aspirins, allergen injection, antacids and antiperspirant etc. (Na et al., 2014; Wilmott et al., 2004; Irimia-Vladu, 2014; Gui et al., 2015), and water purification (Krupińska, 2020). Keeping in view the toxicological effects of aluminum, its toxicity leads to critical impairments and may become a cause of life threatening disease such as Alzheimer's disease, amyotrophic lateral sclerosis (ALS), memory loss, Parkinson's disease, gastrointestinal problems and osteoporosis (Perl and Brody, 1980; Fasman, 1996; Walton, 2006; Perlmutter et al., 1997; Polizzi et al., 2002, Krewski et al., 2007; Skalny et al.; 2021; Maya et al., 2016). The World Health Organization (WHO) recommends that the allowable weekly tolerance of Al^{3+} intake for a human body is *ca.* 7 mg kg^{-1} body weight (Weller et al., 2010).

Carbazole with a rigid fused-ring structure has a nitrogen atom carrying a free electron pair, which forms n–π conjugation with benzene rings (Grabowski et al., 2003). Carbazole possess many benefits, such as good co-planarity along the conjugated system, suitability to structural alterations, strong intramolecular charge-transfer, excellent solubility and stability. Although carbazole and its derivatives are utilized over a wide area, such as electro generated chemiluminescence, solar energy collectors and nonlinear optical materials (Zhu et al., 2011; Yin et al., 2021; Yoon et al., 2007), the research about their use as fluorescent chemosensors is feeble (Yang et al., 2013; Danjou et al., 2012; Fei et al., 2015; Zhu et al., 2015; Qu et al., 2017). 2-Hydroxy-1-naphthaldehyde is substantiated to be a fluorescent building block for the synthesis of distinct fluorescent ligands. The chemo selectivity of the Schiff base ligands including 2-hydroxy-1-naphthaldehyde moiety towards various ions is due to the presence of both hydroxyl group at the *ortho* position and -C = N- bond (Das and Goswami, 2017).

Based on aforementioned explanations, the detection of Al^{3+} has been extremely important in searching its concentration levels in the biosphere and also defining its influences on human health. Through this study, we presented the synthesis of a fluorescent turn on chemosensor for specifying biologically and environmentally significant Al^{3+} ions. Schiff base derivatives are intriguing compounds for sensing of metal ions as well as anions due to guest binding moieties. Schiff base sensor, derived from carbazole and 2-Hydroxy-1-naphthaldehyde units, could be easily prepared in one step. Besides, most of the reported Al^{3+} sensors, which needed complicated synthesis procedures, were insoluble in polar solvent (Chen et al., 2013).

Since the analysis in a high water content solvent was more convenient, the water content was 50% for the complete dissolution of the synthesized Schiff base in this study. The Al^{3+}-sensing mechanism was proposed and provided by the mass spectral and Job's plot analysis. The synthesized ligand depicted high selectivity for Al^{3+} sensing in the presence of multiple ions in ethanol: water (1:1, v/v) mixture. The presumption from the synthesis of carbazole-based Schiff base would exhibit turn-on fluorescence upon binding of aluminum ions with high quantum efficiency in aqueous solution.

2. Experimental part

2.1. Chemicals

Ethylenediaminotetraacetic acid disodium salt dihydrate (Na$_2$-EDTA), the solvents, the metal salts and the sodium salts of F$^-$, Cl$^-$, Br$^-$, I$^-$, CO$_3^{2-}$, HCO$_3^-$ and HPO$_4^{2-}$ ions were purchased from Merck Chemical Co (Germany). CrCl$_3$ was obtained from Riedel-de Häen (Germany). 2-hydroxy-1-naphthaldehyde, 9-ethyl-9*H*-carbazol-3-amine PbCl$_2$, SnCl$_2$·2H$_2$O, K$_2$Cr$_2$O$_7$ and tetrabutylammoniumhexafluorophosphate (TBAPF$_6$) were supplied by Sigma Aldrich (Germany). All chemical reagents procured from commercial suppliers were used without purification in the synthesis and measurements.

2.2. Synthesis of Schiff base (L) and structural characterization

The condensation reaction between 9-ethyl-9H-carbazol-3-amine (0.21 g, 1 mmol) and 2-hydroxy-1-naphthaldehyde (0.172 g, 1 mmol) in a 100 mL flask containing 15 mL of EtOH was maintained for 5 h at 60 °C under reflux with continuous stirring. Then, the solvent was evaporated, and the product of 1-(((9-ethyl-9H-carbazol-3-yl)imino)methyl)naphtalen-2-ol was dried in vacuum to obtain an orange solid (yield 86%). The ligand was abbreviated as L. The synthesis procedure of L was shown in Scheme 1.

FT-IR (cm^{-1}): 3319v (O–H stretching), 3053–2962 v(aromatic C–H stretching), 2918–2865 (aliphatic C-H stretching), 1613 (C = N), 1543, 1488 v(C = C, aromatic ring), 1323 v (C-N, aromatic amine stretching), 1232 v(C-O stretching). ^{1}H NMR (DMSO d_6 δ_H ppm, 9.83 (s, –O$\underline{H}$), 8.56 (–C$\underline{H}$ = N-), 8.56 (d, Hg), 8.26 (d, Ha), 7.90 (d, Hj), 7.79 (d, Hk, Hn), 7.76 (d, Hf)), 7.72 (d, He), 7.62 (d, Hd), 7.56 (t, Hm), 7.48 (t, Hl), 7.35 (t, Hc), 7.23 (t, Hb), 7.05 (d, Hi), 4.48 (q, –C$\underline{H_2}$), 1.32 (t, –C$\underline{H_3}$). ^{13}C NMR (DMSO d_6): δ ppm, 163.23 (C7), 153.09 (C1), 150.42 (C3), 130.26 (C10), 129.56 (C9), 129.41 (C4), 122.23 (C5), 122.11 (C8), 121.55 (C2), 121.29 (C6). ^{13}C NMR (150 MHz, DMSO d_6, δ (ppm)) δ: 159.61, 149.28, 143.01, 140.22, 140.73, 139.72, 139.72, 138.44, 137.12, 132.83, 129.78, 128.00, 125.71, 125.99, 125.21, 122.41, 122.20, 116.96, 115.55, 112.76, 110.23, 59.45, 14.20. LC-MS/MS, m/z: [M + H]$^+$ for L, calc.: m/z = 364, found: m/z = 365 [M + H]$^+$. LC-MS/MS, for L-Al^{3+}, calc.: M = 409, found: M = 410 [M + Al$^{(III)}$ + H$_2$O + H]$^+$.

2.3. Stock solution preparation and instrumentation

1.0×10^{-4} mol L^{-1} solution of L (0.0364 g, 1.0 mol) was prepared in EtOH. 5.0×10^{-3} mol L^{-1} solutions of K$^+$, Ag$^+$, Ba^{2+}, Mn^{2+}, Mg^{2+}, Sn^{2+}, Hg^{2+}, Ca^{2+}, Co^{2+}, Zn^{2+}, Cu^{2+}, Ni^{2+}, Pb^{2+}, Al^{3+}, Fe^{3+}, Cr^{3+} and Cr^{6+} were prepared by solubilizing the metal salts and anions in deionized water. The anions, F$^-$, Cl$^-$, Br$^-$, I$^-$, CO$_3^{2-}$, HCO$_3^-$ and HPO$_4^{2-}$ (1 mM) solutions were also prepared in deionized water. The UV–vis and fluorescence selectivity experiments were performed by taking 1.5 mL of L (1.0 × 10–4 M) and 1.5 mL of different metal ions and anions (5.0 × 10^{-3} M) in a quartz cell to maintain the solvent ratio EtOH:H$_2$O (1:1, v/v).

Characterization studies consisted of the Perkin Elmer Frontier FT-IR Fourier Transform Infrared spectroscopy method using Attenuated Total Reflection accessory for functional groups analysis between 4000 cm^{-1} and 450 cm^{-1}, ^{1}H-600 MHz and ^{13}C NMR-150 MHz spectroscopy with Agilent technologies (DMSO d_6: solvent and TMS: internal standard),

UV–Vis spectroscopy with Analytikjena Specord 210 Plus spectrophotometer, PL emission spectra with Shimadzu R5301 PC spectrofluorophotometer equipped with a Xenon lamp as the excitation source and CV measurements with CHI 660C Electrochemical Analyzer (USA). Optical band gap (E_g) was obtained using the formula of 1242/λ_{onset} (eV) (Colladet et al., 2004). Mass spectrometry data were measured using Finnigan LCQ ion-trap mass spectrometer (Shimadzu LC-MS/MS-8040, Japan). Ligand and ions were combined in a mixture of EtOH: H$_2$O (1:1, v/v).

2.4. Fluorescence spectroscopic study

Photoluminescence (PL) emission spectrum of the ligand (L) in EtOH was monitored by spectrofluorophotometer. Upon addition of K$^+$, Ag$^+$, Ba^{2+}, Mn^{2+}, Mg^{2+}, Sn^{2+}, Hg^{2+}, Ca^{2+}, Co^{2+}, Zn^{2+}, Cu^{2+}, Ni^{2+}, Pb^{2+}, Al^{3+}, Fe^{3+}, Cr^{3+}, Cr^{6+}, F$^-$, Cl$^-$, Br$^-$, I$^-$, CO$_3^{2-}$, HCO$_3^-$ and HPO$_4^{2-}$, the fluorescence spectral behavior was monitored to study influences of the metal ion and anion. A series of Al^{3+} solution (in the range of 0.25 mM-0.195 μM) was prepared on account of observing the concentration efficacy of Al^{3+} ions on the PL property of L.

Fluorescence PL quantum yield (QY_s) is defined as the ratio of the number of photons emitted to the number of photons absorbed through fluorescence of the fluorophore can be determined using the comparative method according to equation (1) (Lakowicz, 1999):

$$QY_s = \frac{A_f F_s n_s^2}{A_s F_f n_f^2} QY_f \tag{1}$$

where A, F and n denote absorption at the maximum excitation wavelength, integrated area underneath the fluorescence emission spectrum and refractive index of the solvent, respectively. Excitation and emission slit width values for both the sample and the standard were adjusted as 5 nm. The fluorescence quantum yield of standard fluorophore was measured using fluorescein in 0.1 M of aqueous NaOH (QY_f = 0.97).

3. Results and discussion

3.1. Structural characterization

Solubility test for the ligand synthesized was carried out at room conditions (L/solvent, 1 mg 1 mL^{-1}). L was soluble in EtOH, DMSO, ethyl acetate, acetonitrile, and acetone, whereas partly soluble in MeOH. In addition, L was insoluble in toluene and hexane as apolar solvent.
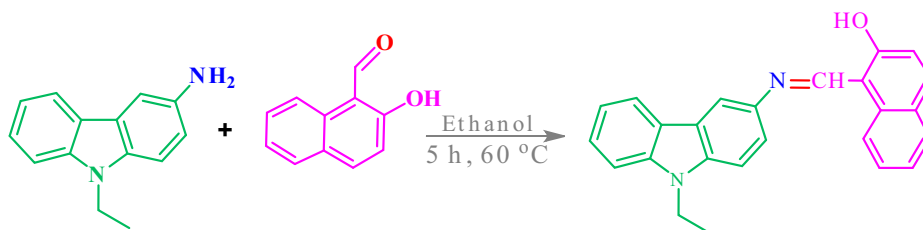
Scheme 1 Synthesis of Schiff base (Ligand = L).

FT-IR and spectroscopy verified the synthesized Schiff base's characteristic substituents. The signal at 3319 cm^{-1} was associated with O-H stretching mode (Fig. S1). The aromatic C-H and the aliphatic C-H stretching vibrations were monitored in the region of 3053–2962 cm^{-1} and 2918–2865 cm^{-1}, respectively. In the IR spectrum of L, absence of the peak related to the amine group (–NH$_2$) and the peak for the aldehyde carbonyl group (-C = O) indicated the formation of a Schiff base compound, with concomitant characteristic stretching vibration pronounced at 1613 cm^{-1} for the imine (–HC = N-) group. The peaks observed at 1543 cm^{-1} and 1488 cm^{-1} were attributed to the vibration bands of C = C bonds in the benzene ring. The C-N and C-O stretching modes were noticeable at 1323 cm^{-1} and 1232 cm^{-1}, respectively. The sharp peaks between 807 cm^{-1} and 719 cm^{-1} could be related to the C = C and C-H bending modes.

^{1}H NMR spectra of the Schiff base (L) and the coordinated L with Al^{3+} are displayed in Fig. S2. The peaks at 9.83 ppm and 8.56 ppm were attributed to –OH and –CH = N- protons of L, respectively. The aromatic protons of L were observed between 8.56 ppm and 7.05 ppm. Owing to the positive mesomeric effect of –OH group, the *ortho* positioned Hi came out up field at 7.05 ppm as doublet and the *meta* positioned Hj moved downfield to 8.07 ppm as doublet (Fig. S2a). The signals of the protons in the aliphatic region were observed at 4.48 ppm (quartet) and 1.32 ppm (triplet) for –CH$_2$ and –CH$_3$, respectively. Slight changes in the δ values upon coordination with Al^{3+} ions were depicted in Fig.S2b. Since the coordination took place from both –OH and –CH = N- sides, the regarding protons of –OH and –CH = N- moved up field and recorded shift of Δδ 0.09 ppm and Δδ 0.14 ppm, respectively. A lowered intensity for the –OH peak was observed. Aromatic protons showed slightly up field shift upon chelation. It could be inferred that the binding of L to Al^{3+} resulted in a formation of a rigid system along with imine-nitrogen and hydroxyl group of L as binding site.

^{13}C NMR spectrum of the synthesized Schiff base (L) is displayed in Fig.S3. The highest chemical shift value of azomethine carbon (–CH = N-) appeared at 169.83 ppm. Since –OH group of naphthyl moiety pulled electrons away from the ring inductively, the peak of C14 was deshielded to 154.28 ppm. Due to the electronegative element of nitrogen, C1 of carbazole moiety also appeared downfield at 140.69 ppm. The aromatic carbons were observed in the range of 138.84–109.06 ppm. Alkyl –CH$_2$ and –CH$_3$ asserted themselves at 37.66 ppm and 14.13 ppm, respectively. In consideration of (+) mesomeric effect of OH group towards the ring inducing a negative charge formation at the *ortho* and *para* corners of the naphthyl moiety, the peaks at 129.1 ppm, 120.75 ppm and 109.92 ppm were attributed to C17, C15 and C13, respectively. The peak of the *meta* positioned C16 was observed at 138.85 ppm. C3 and C7, which were the *ortho* and *para* positioned carbons appeared at 126.78 and 115.19 ppm, respectively. ^{1}H NMR was integrated with ^{13}C NMR spectral measurement for the structural confirmation of L.

Fig. 1 shows the optical behavior of L recorded by UV–vis spectroscopy. The optical measurements were implemented at room temperature in the range of 260–800 nm, versus a blank solution in EtOH:H$_2$O (1:1). The normalized absorption spectrum of the free sensor L displayed three absorption bands
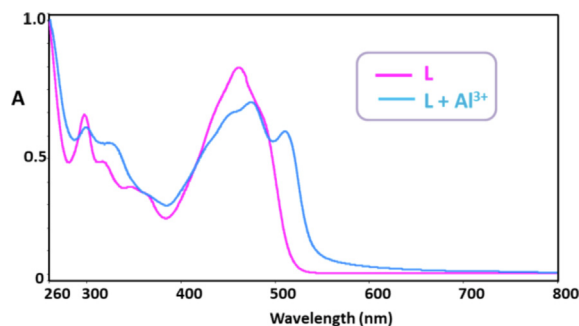

Fig. 1 UV–vis absorption spectra of L (0.1 mM) and L + Al^{3+} (0.5 mM) in EtOH.

centered at 297 nm, 318 nm and 330 nm, corresponding to the intra-ligand aromatic π → π* electron transitions. The prominent band of L displayed at 462 nm could be ascribed to the electronic transitions from nonbonding orbitals on the heteroatoms to ligand π* orbitals, namely, n → π* electronic transition. Upon addition of Al^{3+} ions, the absorption bands of aromatic π → π* electron transitions were observed at 298 nm, 318 nm and 330 nm. The absorption band at a maximum wavelength of 462 nm indicated a bathochromic shift to 479 nm. A new band at 531 nm arose upon complexation with Al^{3+} in EtOH:H$_2$O (1:1, v/v) via the donation of lone pairs of electrons on nitrogen/oxygen of the ligand to metal ion charge transfer. λ$_{onset}$ is the onset wavelength which can be identified by intersection of two tangents on the absorption edges, indicating the starting wavelength for the electronic transition (Colladet et al., 2004). λ$_{onset}$ values obtained from the UV–Vis spectra were obtained as 519 nm and 580 nm, respectively. The calculated optical band gap (E_g) value of L was 2.39 eV in EtOH:H$_2$O. Having coordinated to Al^{3+} ions, this value lowered to 2.14 eV as a result of a chelation between L and Al^{3+}. Bathochromic shift observed in UV–vis spectra was ensued from the binding of Al^{3+} ions to -C = N- bridge and –OH of 2-hydroxynaphthalene unit (Das and Goswami, 2017; Yoon et al., 2007). On account of charge transfer from L towards Al^{3+}, the yellow solution of L turned into white upon addition of Al^{3+} ions under 366 nm of UV light, as shown in Fig. 2. The addition of other metal ions and anions (K$^+$, Ag$^+$, Ba^{2+}, Mn^{2+}, Mg^{2+}, Sn^{2+}, Hg^{2+}, Ca^{2+}, Co^{2+}, Zn^{2+}, Cu^{2+}, Ni^{2+}, Pb^{2+}, Al^{3+}, Fe^{3+}, Cr^{3+}, Cr^{6+}, F$^-$, Cl$^-$, Br$^-$, I$^-$, CO$_3^{2-}$, HCO$_3^-$ and HPO$_4^{2-}$) did cause no alterations on metal-complexation, which was also confirmed by detecting no color change under 366 nm light, as seen in Fig. 2A and Fig. 2B.

3.2. pH effect

To determine useful pH range where the ligand can perform without being affected by hydrogen ions, which cause interference in the performance of the ligand is necessary. Thus, pH dependence of the ligand was investigated and the results obtained are given in Fig. 3. The emission intensity of L (0.1 mM) was stable in the pH range from 2.0 to 12.0, concluding with a pH-independent ligand. Being present of Al^{3+} (20 eqv.) enhanced the PL emission intensity, which reached to maximum value at midpoint, therefore, it was better to make all measurements at pH 7.5 and 8.0 (Fig. 3). The change in potential above pH 8.0 resulted in the formation of Al(OH)$_3$
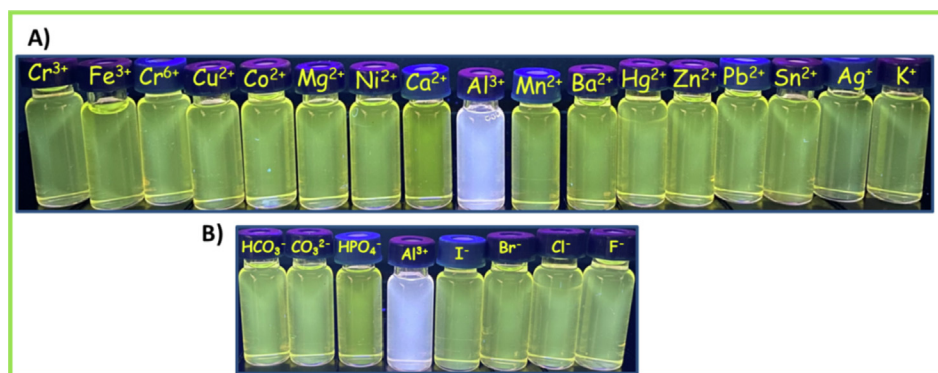
Fig. 2 Digital camera photograph of L in the presence of metal ions (A) and anions (B) under 366 nm UV light.

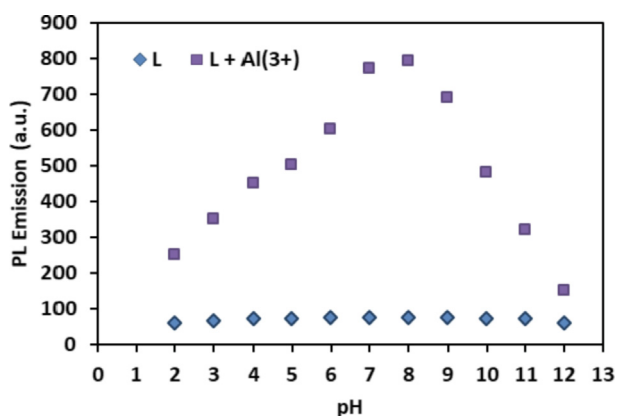**Fig 3** pH dependence of L and L + Al^{3+}.

concomitant with the breakdown of L-Al^{3+} complex, hence fluorescence was quenched. Consequently, L could be used for sensing Al^{3+} ions in aqueous medium under neutral conditions.

3.3. Selectivity of L to Al^{3+} and competitive study

The selectivity of L (0.1 mM) in EtOH was investigated towards metal ions (K^+, Ag^+, Ba^{2+}, Mn^{2+}, Mg^{2+}, Sn^{2+}, Hg^{2+}, Ca^{2+}, Co^{2+}, Zn^{2+}, Cu^{2+}, Ni^{2+}, Pb^{2+}, Al^{3+}, Fe^{3+}, Cr^{3+} and Cr^{6+}, 1.0 eqv. in H_2O) and anions (F^-, Cl^-, Br^-, I^-, CO_3^{2-}, HCO_3^- and HPO_4^{2-}, 1.0 eqv. in H_2O). The sensor L possessed a weak fluorescence emission at 533 nm with 73 a. u. intensity under excitation at 320 nm. The excited-state intramolecular proton transfer (ESIPT) eventually the phenolic proton and C = N isomerization, resulting in non-fluorescent ligand (Tang et al., 2011; Chen et al., 2021). It was noted that only Al^{3+} ion exhibited a drastic enhancement in the PL emission spectra. The excitation at 320 nm gave results for the emission intensities of L-metal ion and L-anion solutions in the presence of K^+, Ag^+, Ba^{2+}, Mn^{2+}, Mg^{2+}, Sn^{2+}, Hg^{2+}, Ca^{2+}, Co^{2+}, Zn^{2+}, Cu^{2+}, Ni^{2+}, Pb^{2+}, Al^{3+}, Fe^{3+}, Cr^{3+}, Cr^{6+}, F^-, Cl^-, Br^-, I^-, CO_3^{2-}, HCO_3^- and HPO_4^{2-}, which were found to be 74, 98, 78, 73, 101, 102, 79, 102, 101, 96, 103, 96, 95, 789, 39, 104, 74, 82, 78, 77, 91, 91, 92 and 91 a.u, respectively, at 533 nm of maximum emission wavelength of L as displayed in Fig. 4. All of the emission bands exhibit the same spectral envelope. As demonstrated in Fig. 4, the fluorescence enhancement performance in the

presence of Al^{3+} observed at 533 nm was 11-fold greater than that of the control by emitting white color, indicating that L came up with a high fluorescent selectivity towards Al^{3+}, while no fluorescence was monitored in the presence of other metal ions and anions.

Due to the isomerization of the C = N bond in the excited state via the excited state intra molecular proton transfer (ESIPT) (Manna et al., 2020), the ligand showed weak fluorescence. Specific metal ion binding through O donor site and the C = N moiety of L restricted C = N isomerization and thus, emission intensity could be enhanced due to the chelation enhancement fluorescence (CHEF) effect (Gupta and Kumar, 2016). The participation of Al^{3+} in the ethanol solution of L eventuated with an emission enhancement at 533 nm due to chelation-enhanced fluorescence (CHEF) (Kim et al., 2003) on account of binding with Al^{3+}, which could be related to the formation of a rigid system by the coordination of Al^{3+}, leading to the disruption of the ESIPT feature (Salarvand et al., 2019; Li et al., 2013). The fluorescence enhancement happens due to the non-bonded electrons of N atom from C = N took part in coordination with Al^{3+} ion to inhibit the isomerization process. The coordination of L with Al^{3+} ion hindered the rotation around the C = N bond and prevented the C = N isomerization. The result was the inhibition of ESIPT in the ligand, resulting in a fluorescence enhancement and inducing chelation-enhanced fluorescence, thereby generating white fluorescence in the ligand–metal product. The selectivity and sensitivity took part in fluorescence enhancement by Al^{3+} ion capturing and the PL emission change through CHEF effect (Sahana et al., 2013; Shyamal et al., 2016; Manna et al., 2020; Shyamal et al., 2016) due to retardation of C = N isomerization. The presence of C = N and O sites of L, which showed strong affinity towards a hard metal like Al^{3+}, would form the chelation with Al^{3+} and, thus, would be the essence of a promising turn-on fluorescent sensor for Al^{3+} ion, as seen in Fig. 5.

The fluorescence quantum yield (QY) of L-Al^{3+} system was calculated as 21.3%. Time-dependent (0–3600 sec) fluorescence measurement pointed out that irradiation at 320 nm within 3600 sec eventuated with no considerable changes in fluorescence emission intensity as displayed in Fig.S4, showing that the L-Al^{3+} system possessed a remarkable photostability in EtOH:H_2O (1:1, v/v) media.

To further corroborate the high selectivity of L sensor towards Al^{3+}, competitive tests were conducted in the pres-
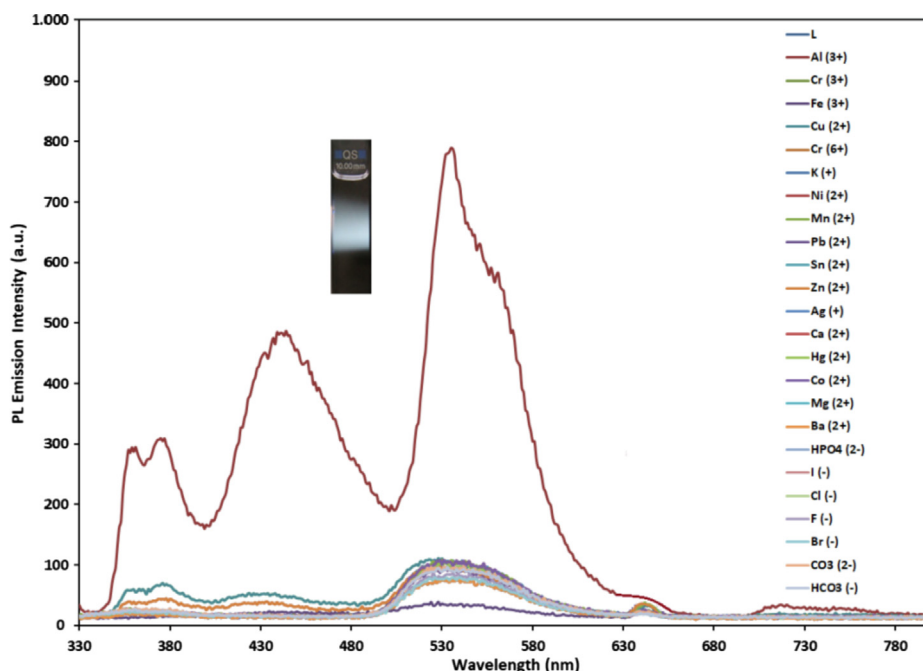
Fig. 4 Fluorescence emission spectra of L (0.1 mM) treatment with various metal ions and anions such as Ag^+, K^+, Mg^{2+}, Ba^{2+}, Mn^{2+}, Hg^{2+}, Sn^{2+}, Co^{2+}, Ca^{2+}, Ni^{2+}, Cu^{2+}, Zn^{2+}, Pb^{2+}, Al^{3+}, Fe^{3+}, Cr^{3+}, Cr^{6+}, F^-, Cl^-, Br^-, I^-, CO_3^{2-}, HCO_3- and HPO_4^- (0.5 mM) at room temperature in EtOH: H_2O (1:1, v:v, λ_{ex} = 320 nm, excitation and emission slit widths = 5 nm).
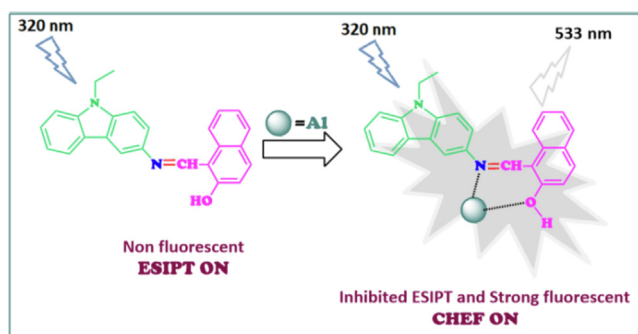

Fig. 5 Suggested mechanism of binding of L with Al^{3+}.

ence of selected metal ions and anions. The selectivity of L towards Al^{3+} was examined in a ternary mixture containing L (0.1 mM), Al^{3+} (0.5 mM) and other interfering metal ions

(K^+, Ag^+, Ba^{2+}, Mn^{2+}, Mg^{2+}, Sn^{2+}, Hg^{2+}, Ca^{2+}, Co^{2+}, Zn^{2+}, Cu^{2+}, Ni^{2+}, Pb^{2+}, Al^{3+}, Fe^{3+}, Cr^{3+} and Cr^{6+}, 0.5 mM) and anions (F^-, Cl^-, Br^-, I^-, CO_3^{2-}, HCO_3- and HPO_4^{2-}, 0.5 mM), followed by excitation at 320 nm. Fig. 6 and Fig. 7 revealed that the fluorescence intensity of L-Al^{3+} at 533 nm had no obvious fluorescent alterations in the presence of the other metal ions and anionic species, concluding with the fact that the tested ions had no prominent impact on fluorescence intensity of the L-Al^{3+} system.

3.4. Fluorescence titration study and limit of detection (LOD) of aluminum ions

Non-fluorescence property of the ligand (L) was altered by the addition of Al^{3+} to the yellow colored L solution resulting in a bright white fluorescence under excitation at 320 nm. The flu-
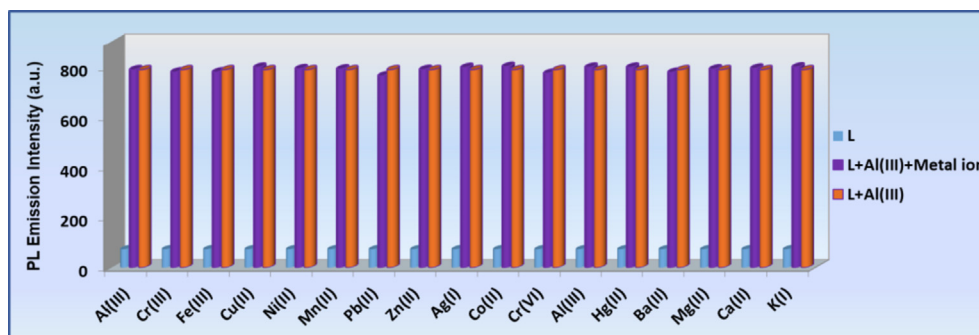

Fig. 6 (blue bar): metal ion selectivity profile of the sensor L (0.1 mM); (orange bar): change in emission of L + Al^{3+} (0.5 mM); (purple bar): change in emission of L + Al^{3+} + M^{n+} (0.5 mM) at 533 nm.
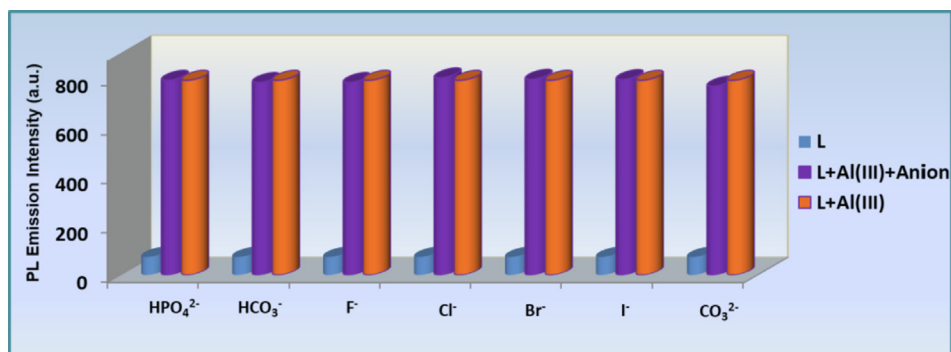
Fig. 7 (blue bar): anion selectivity profile of the sensor L (0.1 mM); (orange bar): change in emission of L + Anion^{n-} (0.5 mM); (pruple bar): change in emission of L + Al^{3+} + Anion^{n-} at 533 nm.
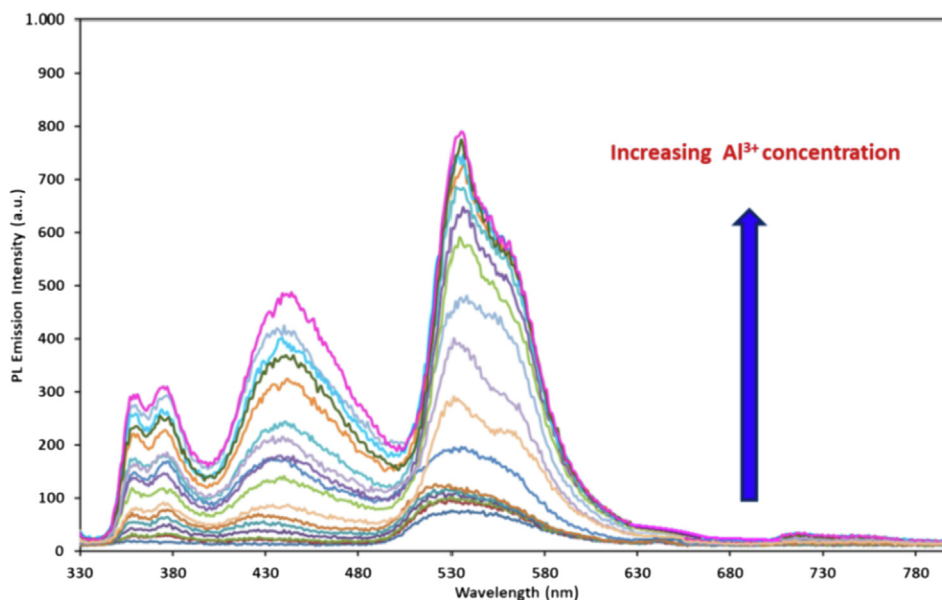

Fig. 8 Fluorescence emission spectra recorded for L (0.1 mM) upon increasing concentration of Al^{3+} ion (2.50×10^{-4}, 2.25×10^{-4}, 1.75×10^{-4}, 1.50×10^{-4}, 1.25×10^{-4}, 1.0×10^{-4}, 5.0×10^{-5} 1.25×10^{-5}, 6.125×10^{-6}, $3,125 \times 10^{-6}$, $1,56 \times 10^{-6}$, 7.8×10^{-7}, 3.9×10^{-7}, 1.95×10^{-7} M).

orescence titration of L upon the addition of different concentrations of Al^{3+} from 0.25 mM to 0.195 µM at 533 nm of an emission wavelength revealed an increase in the fluorescence emission intensity, as seen in Fig. 8.

To make a detailed investigation about the binding mode, limit of detection (LOD) of L for Al^{3+} was determined using fluorescence titration results. Fig. 9 represents the fluorescence emission intensity of L (I) in the presence of Al^{3+} at 533 nm versus the concentration of Al^{3+} ions ranged from 0.25 mM to 0.195 µM. From the changes in Al^{3+} dependent fluorescence intensity ($I_{533 \text{ nm}}$), the LOD in EtOH:H$_2$O (1:1, v/v) was estimated to be 2.59×10^{-7} M, using the formula of LOD = 3σ/k formula (Analytical Methods Committee, 1987), where σ was standard deviation of ten control measurements of L, and k was the slope of the line created by plotting the fluorescence intensities versus [Al^{3+}] values. The calculated LOD value was below the tolerable concentration of Al^{3+} in drinking water (2.41 µM) as defined by WHO, and Al^{3+} levels higher than 2.4 µM may cause encephalopathy as reported in
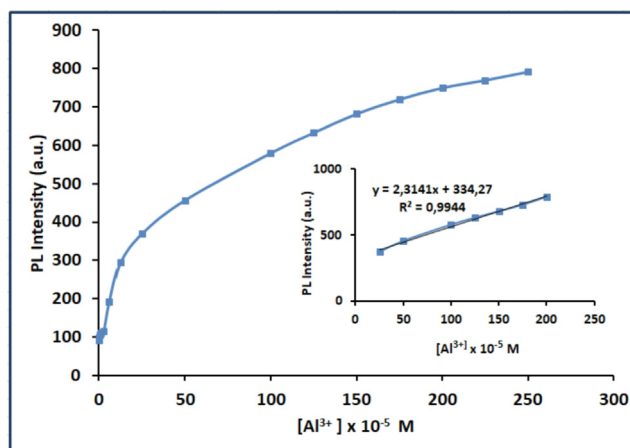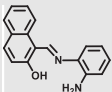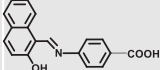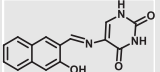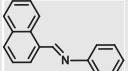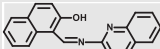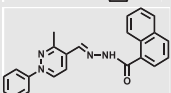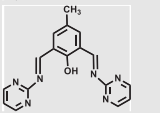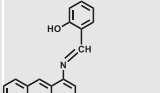

Fig. 9 Plot of the fluorescence intensity at the PL emission peak of L at 533 nm versus the concentration of Al^{3+} (0.25 mM – 0.195 µM).

Table 1 Comparison of same Schiff base ligands for the selectivity of Al^{3+}.

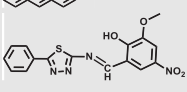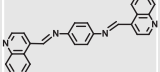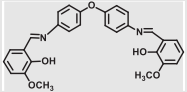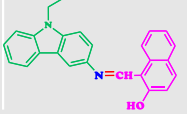| Structure of chemosensor	Media	LOD (mol L^{-1})	Ka (M^{-1})	Reference
	EtOH/HEPES buffer (95:5, v/v)	1.08×10^{-7}	6.53×10^3	(Zhu et al., 2016)
	MeOH-H_2O (9:1 v/v)	6.4×10^{-7}	1.546×10^5	(Salarvand et al., 2019)
	CH_3CN	3.2×10^{-7}	3.148×10^4	(Singh et al., 2013)
	MeOH-H_2O (1:1 v/v)	5.0×10^{-5}	4.0×10^6	(Kumar et al., 2015)
	CH_3CN: H_2O (1:1, v:v)	1.98×10^{-6}	4.35×10^4	(Huang et al., 2017)
	EtOH/ H_2O (1:1, v:v)	2.2×10^{-7}	1.89×10^4	(Wang et al., 2015)
	H_2O:DMSO (1:9, v/v)	1.27×10^{-6}	6.4×10^4	(Roy et al, 2021)
	MeOH-H_2O	5.2×10^{-6}	1.05×10^4	(Kaur and Kaur, 2017)
	MeOH-Tris-HCl buffer (1:1, v/v)	1.15×10^{-7}	$1.76 \times 10^2\ M^{-1/2}$	(Manna et al., 2020)
	MeOH-water (2:1, v/v)	1.26×10^{-8}	1.23×10^5	(Ghorai et al., 2016)
	CH_3CN: H_2O (1:1, v:v)	1.17×10^{-7}	2.35×10^5	(Chandra et al., 2020)
	EtOH/deionized H_2O (1:1, v/v)	2.59×10^{-7}	5×10^4	This study

the literature (Kaur, and Kaur, 2017), indicating that L was highly sensitive to the recognition of Al^{3+} ions at the submicromolar concentration.

Some reported similar studies about Schiff base sensors for the recognition of Al^{3+} and the calculated LOD, K_a values are arranged in Table 1. Based on the aforementioned findings, low LOD value of L for Al^{3+} specified that the Schiff base synthesized in this study demonstrated a distinctive selectivity compared to other Schiff base ligands sensing aluminum in the literature (Roy, 2021; Salarvand et al., 2019; Kaur, and Kaur, 2017; Zhu et al., 2016; Singh et al., 2013; Kumar et al., 2015; Huang et al., 2017; Wang et al., 2015, Manna et al., 2020; Ghorai et al., 2016; Chandra et al. 2020). Although Schiff base sensor with 2-hydroxy-1-benzaldehyde and anthracene moieties possessed a fluorescence response towards both Hg (II) and Al (III) in the presence of interfering metal ions (Kaur, and Kaur, 2017), the ligand synthesized in this study formed a chelate between only Al (III) in the presence

of competing metal ions and anions, indicating a specific selectivity of L. The lowest LOD value for the Schiff base chemosensor synthesized by Ghorai et al. had a fluorescence response towards both Hg (II) and Al (III) (Ghorai et al., 2016). Another Schiff base containing pyrene and *o*-vanillin units synthesized by Shyamal et al. had 8.64 nM of LOD for Al^{3+} in CH_3CN: H_2O (95:5, v:v) (Shyamal et al., 2016a).

Since the analysis of an analyte in a high water content solvent was more suitable for the analysis of real samples, the water content was 50% for the complete dissolution of the synthesized Schiff base in this study.

3.5. Binding affinity of L towards Al^{3+}

A meticulous study was carried out to comprehend the binding behavior of L towards Al^{3+} ions using Job's plot analysis based on fluorescence measurement (Likussar and Boltz, 1971; Job, 1984). In this method, standard nine mixtures were
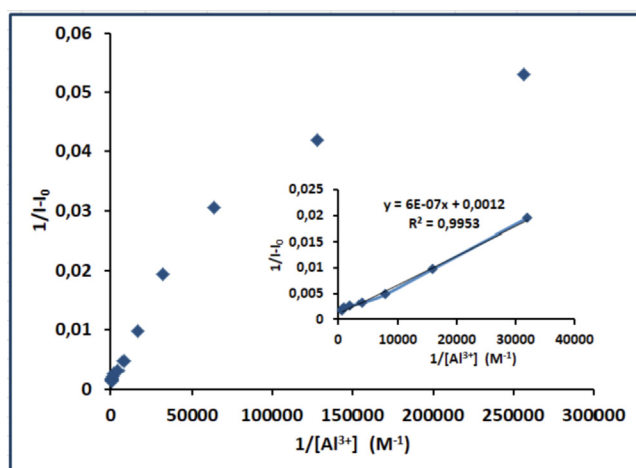
Fig. 10   Benesi-Hildebrand plot of $1/I-I_0$ versus $1/[Al^{3+}]$.

prepared by adding aliquots of Al^{3+} equivalent to 9–1 μmol into a series of 10 mL volumetric flasks containing aliquots of L equivalent to 1–9 μmol so that each flask contained a total number of 10 μmol. Job's plot was acquired by plotting PL emission values at 533 nm versus the mole fraction of ligand (L) where the transition point for fluorescence intensity was observed at the molar fraction of 0.5, specifying that 1:1 stoichiometric complexation of L with Al^{3+} (Fig. S5). To support 1:1 binding mode, LC-MS/MS of L and L + Al^{3+} were presented. The LC-MS/MS spectrum of L revealed an intense peak at m/z 365 corresponding to $[L + H]^+$ (Fig S6). Upon addition of 20 eqv. of Al^{3+}, a main peak at m/z 410 appeared and could be assignable to the 1:1 formation of $[L + Al (III) + H_2O + H]^+$ (Fig. S7). Al^{3+} used two 3-level orbitals to make chelation with L and one 3-level orbital to accept lone pair from one water molecule. The result was to obtain an isotopic peak at m/z 410 of $[L + Al (III) + H_2O + H]^+$.

The calculation of the binding constant (K_a) for the L + Al^{3+} chelation was obtained according to Benesi-Hildebrand expression (Benesi and Hildebrand, 1949). Fluorescence titration study provided a plot for the calculated values of $[1/(I-I_0)]$ at 533 nm depending on $1/[Al^{3+}]$, as seen in Fig. 10. The slope of the line drawn by using Benesi–Hildebrand equation led us to calculate the association constant (K_a) of the L + Al^{3+} complex, which was found to be $5 \times 10^4 M^{-1}$. I and I_0 were the fluorescence emission intensities

of L in the presence and in the absence of Al^{3+} ion, respectively.

3.6. Reversibility process using electrochemical techniques

The reversibility of the chemosensor to target ion binding is a very important aspect in practical application. Accordingly, the reversibility of L + Al^{3+} chelation was studied using electrochemical techniques (Patil et al., 2019). To estimate oxidation–reduction behavior of L, redox behavior was investigated by the cyclic voltammetry (CV) technique with a predictable three-electrode cell assembly with Pt wire as counter-electrode, glassy carbon as a working electrode and Ag/AgCl as the reference electrode. The supporting electrolyte was 0.1 M $TBAPF_6$ in acetonitrile solution. The CVs were monitored at a scan rate of 100 mV s^{-1} in the potential range from + 2.0 V to -2.0 V to detect peaks in both forward and reverse scans at room temperature and under Argon atmosphere. Two quasi-reversible oxidation CV waves representing the oxidation–reduction process were apparent in Fig. S8. The HOMO-LUMO energy levels and the calculated band gap values are tabulated in Table 2. Initial oxidation corresponded to carbazole oxidation at a potential of 1.15 V, forming the cation radical (polaron) in one-electron process (Karon and Lapkowski, 2015). The first oxidation peak was reversible. Since each discrete oxidation process was also assigned to a unique one-electron transfer, the other oxidation then formed at around 1.54 V associated with hydroxyl group, forming polaron structure when scanning to higher anodic potentials (E_{pa}) (Seo et al., 1966). The cathodic reduction peak (E_{pc}) of L, seen at -1.55 V, was due to the reduction process observed via protonation of azomethine nitrogen of C = N linkage (Kolcu and Kaya, 2016). The HOMO and LUMO energies designating the ability to donate an electron and the capability to accept the electron were calculated using the formulas of $E_{HOMO} = -(4.39 + E_{pa})$ eV and $E_{LUMO} = -(4.39 + E_{pc})$, respectively. To gain knowledge about the electron transition to take place in the ligand and in the ligand-Al^{3+} complex, the calculation of band gap (E'_g) energy between HOMO and LUMO was fulfilled. The energy gap had control over the electron transition to occur in the ligand and in the ligand bound to metal ion. E'_g was found to be 3.10 eV and decreased to 2.52 eV after addition of Al^{3+} ion, concluding with the fact that the formation of L + Al^{3+} system lowered the energy required for the electronic transition. These results were also in conformity with the result obtained from UV–vis spectral

Table 2   CV results of L and L + Al^{3+}.

Compound	$^aE_{ox}$ (eV)	$^bE_{red}$ (eV)	^cHOMO (eV)	^dLUMO (eV)	$^eE'_g$ (eV)
L	1.5403	−1.5579	−5.93	−2.83	3.10
	1.1504	−0.8365	−5.54	−3.55	
	0.9963				
L + Al^{3+}	1.6144	−0.9275	−6.00	−3.48	2.52
	1.1547				
	0.8992				

^{a} Onset oxidation potential. ^{b} Onset reduction potential.
^{c} Highest occupied molecular orbital. ^{d} Lowest unoccupied molecular orbital.
^{e} Electrochemical band gap.

studies, in which a decrease in the calculated optical band gap (E_g) value of L after coordination to Al^{3+} ions, as a result of a chelation between L and Al^{3+}. The disappearance of the reduction peak of L at -1.55 V, as seen in Fig. 16, in presence of Al^{3+} confirmed that chelation took place between Al^{3+} ions and L. The reversibility feature, which was essential in developing a sensor (Rana et al., 2017), could be tested by titration of L-Al^{3+} complex with 1.0 equivalent of Na_2EDTA, which resulted in the recovery of the original C $=$ N reduction peak of L in the voltammogram, as displayed in Fig. 16. The reappearance of the original -C $=$ N- reduction peak of L revealed that EDTA displaced the metal ion in L-Al^{3+} system, confirming decomplexation of the L-Al^{3+} adduct; in other words, L could be successfully recovered.

4. Conclusion

A Schiff base chemosensor comprising carbazole and 2-hydroxybenzaldehyde moieties was developed for the selective recognition of aluminum ions in aqueous-alcohol medium, coupled with its straightforward synthesis. Simple and inexpensive fluorescent probe exhibited a turn-on fluorescence response toward Al^{3+} at sub micromolar range over other metal ions and anions. The fluorescence enhancement upon formation of sensor-Al^{3+} adduct was observed due to inhibition of C $=$ N isomerization along with ESIPT, concomitantly CHEF effect predominated in the system, which was asserted itself by a prominent color change from yellow to white under UV lamp. Since PL emission spectroscopy was to be seen as supplementary to the optical measurement, fluorescence measurements were conducted for appraising the results. The change in fluorescence intensity was such that the synthesized Schiff base exhibited "turn-on" mode of high sensitivity towards Al^{3+} ions. The fluorescence quantum yield (QY) of L in the presence of Al^{3+} was found to be 21.3% along with presenting an outstanding photostability in 3600 sec under excitation at 320 nm. The limit of detection (LOD) of L and the binding constant (K_a) was found to be 2.59×10^{-7} M and 5×10^4 M^{-1}, revealing a chemosensor, which could detect sub-micromolar concentration of Al^{3+} in aqueous solution along with a stable complex formation of L-Al^{3+}. Keeping in view that the decrease in the band gap energy was observed, the probability of binding ability of L with Al^{3+} increased. The sensing ability and functional reversibility of L could make this sensor appealing to detect Al^{3+} ions. Fluorescence sensing ability of L to detect Al^{3+} ions in aqueous-ethanol environment make it to use as a fluorescent probe in biological imaging in the cells.

Appendix A. Supplementary data

Supplementary data to this article can be found online at https://doi.org/10.1016/j.arabjc.2022.103935.

References

Abu-Dief, A.M., Mohamed, I.M., 2015. A review on versatile applications of transition metal complexes incorporating Schiff bases. Beni-Suef Univ. J. Basic Appl. Sci. 4, 119–133. https://doi.org/10.1016/j.bjbas.2015.05.004.

Analytical Methods Committee, 1987. Recommendations for the definition, estimation and use of the detection limit. Analyst 112, 199–204. https://doi.org/10.1039/AN9871200199.

Arumugam, V., Kaminsky, W., Bhuvanesh, N.S.P., Nallasamy, D., 2015. Palladium (II) complexes containing ONO tridentate hydrazone for Suzuki-Miyaura coupling of aryl chlorides in aqueous-organic media. RSC Adv. 5, 59428–59436. https://doi.org/10.1039/C5RA10973F.

Arunadevi, A., Raman, N., 2020. Biological response of Schiff base metal complexes incorporating amino acids-a short review. J. Coord. Chem. 73, 2095–2116. https://doi.org/10.1080/00958972.2020.1824293.

Bar, F., Hopf, H., Knorr, M., Schroder, O., Krahl, J., 2016. Effect of hydrazides as fuel additives for biodiesel and biodiesel blends on NOx formation. Fuel 180, 278–283. https://doi.org/10.1016/j.fuel.2016.04.028.

Benesi, H.A., Hildebrand, J.H., 1949. A spectrophotometric investigation of the interaction of iodine with aromatic hydrocarbons. J. Am. Chem. Soc. 71, 2703–2707. https://doi.org/10.1021/ac60304a006.

Berhanu, A.L., Gaurav, Mohiuddin, I., Malik, A.K., Aulakh, J.S., Kumar, V., Kim, K.H., 2019. A review of the applications of Schiff bases as optical chemical sensors. Trend. Anal. Chem. 116, 74-91. 10.1016/j.trac.2019.04.025.

Burgess, J., 1996. Man and the elements of group 3 and 13. Chem. Soc. Rev. 25, 85–92. https://doi.org/10.1039/CS9962500085.

Chandra, R., Manna, A.K., Sahu, M., Rout, K., Patra, G.K., 2020. Simple salicylaldimine-functionalized dipodal bis Schiff base chromogenic and fluorogenic chemosensors for selective and sensitive detection of Al^{3+} and Cr^{3+}. Inorg. Chim. Acta 499,. https://doi.org/10.1016/j.ica.2019.119192 119192.

Chang, C.J., Gunnlaugsson, T., James, T.D., Targets, S., 2015. Chem. Soc. Rev. 44, 4176–4178. https://doi.org/10.1039/C5CS90058A.

Chen, C.H., Liao, D.J., Wan, C.F., Wu, A.T., 2013. A turn-on and reversible Schiff base fluorescence sensor for Al^{3+} ion. Analyst 138, 2527–2530. https://doi.org/10.1039/C3AN00004D.

Chen, L., Fu, P.Y., Wang, H.P., Pan, M., 2021. Excited-state intramolecular proton transfer (ESIPT) for optical sensing in solid state. Adv. Opt. Mater. 9, 2001952. https://doi.org/10.1002/adom.202001952.

Colladet, K., Nicolas, M., Goris, L., Lutsen, L., Vanderzande, D., 2004. Low-band gap polymers for photovoltaic applications. Thin Solid Films 451, 7–11. https://doi.org/10.1016/j.tsf.2003.10.085.

Da Silva, C.M., Da Silva, D.L., Modolo, L.V., Alves, R.B., Martins, C.V.B., De Resende, M.A., De Fátima, A., 2011. Schiff bases: A short review of their antimicrobial activities. J. Adv. Res. 2, 1–8. https://doi.org/10.1016/j.jare.2010.05.004.

Danjou, P.E., Lyskawa, J., Delattre, F., Becuwe, M., Woisel, P., Ruellan, S., Fourmentin, S., Cazier-Dennin, F., 2012. New fluorescent and electropolymerizable N-azacrown carbazole as a selective probe for iron (III) in aqueous media. Sensor Actuat. B-Chem. 171, 1022–1028. https://doi.org/10.1016/j.snb.2012.06.027.

Das, A.K., Goswami, S., 2017. 2-Hydroxy-1-naphthaldehyde: A versatile building block for the development of sensors in supramolecular chemistry and molecular recognition. Sensor Actuat. B-Chem. 245, 1062–1125. https://doi.org/10.1016/j.snb.2017.01.068.

Fan, L., Qin, J.C., Li, C.R., Yang, Z.Y., 2020. Two similar Schiff-base receptor based quinoline derivate: Highly selective fluorescent probe for Zn(II). Spectrochim. Acta A 236,. https://doi.org/10.1016/j.saa.2020.118347 118347.

Fasman, G.D., 1996. Aluminum and Alzheimer's disease: model studies. Coordin. Chem. Rev. 149, 125–165. https://doi.org/10.1016/S0010-8545(96)90020-X.

Fei, X.N., Hao, Y.C., Gu, Y.C., Li, C., Yu, L., 2015. Synthesis, photophysical and electrochemical properties of two novel carbazole-based dye molecules. J. Fluoresc. 135, 379–385. https://doi.org/10.1016/j.saa.2014.06.159.

Ghorai, A., Mondal, J., Chowdhury, S., Patra, G.K., 2016. Solvent-dependent fluorescent-colorimetric probe for dual monitoring of Al^{3+} and Cu^{2+} in aqueous solution: an application to bio-imaging. Dalton Trans. 45, 11540–11553. https://doi.org/10.1039/c6dt01795a.

Grabowski, Z.R., Rotkiewicz, K., Rettig, W., 2003. Structural changes accompanying intramolecular electron transfer: focus on twisted intramolecular charge-transfer states and structures. Chem. Rev. 103, 3899–4031. https://doi.org/10.1021/cr940745l.

Gui, S., Huang, Y., Hu, F., Jin, Y., Zhang, G., Yan, L., Zhang, D., Zhao, R., 2015. Fluorescence turn-on chemosensor for highly selective and sensitive detection and bioimaging of Al^{3+} in living cells based on ion-induced aggregation. Anal. Chem. 87, 1470–1474. https://doi.org/10.1021/ac504153c.

Gupta, A., Kumar, N., 2016. A review of mechanisms for fluorescent "turn-on" probes to detect Al^{3+} ions. RSC Adv. 6, 106413–106434. https://doi.org/10.1039/C6RA23682K.

He, H., Cheng, Z., Zheng, L., 2021. Aqueous Zn^{2+} analysis: Specific recognition and instant imaging by Schiff base fluorescent probes. J. Mol. Str. 1227,. https://doi.org/10.1016/j.molstruc.2020.129522 129522.

Hirayama, T., Okuda, K., Nagasawa, H., 2013. A highly selective turn-on fluorescent probe for iron(II) to visualize labile iron in living cells. Chem. Sci. 4, 1250–1256. https://doi.org/10.1039/C2SC21649C.

Huang, P.C., Fang, H., Xiong, J.J., Wu, F.Y., 2017. A highly selective turn-on fluorescent probe for Al^{3+} in aqueous solution based on quinoline Schiff-base. Methods Appl. Fluores. 5,. https://doi.org/10.1088/2050-6120/aa7172 024014.

Iacopetta, D., Ceramella, J., Catalano, A., Saturnino, C., Bonomo, M.G., Franchini, C., Sinicropi, M.S., 2021. Schiff Bases: Interesting scaffolds with promising antitumoral properties. Appl. Sci. 11, 1877. https://doi.org/10.3390/app11041877.

Irimia-Vladu, M., 2014. "Green" electronics: biodegradable and biocompatible materials and devices for sustainable future. Chem. Soc. Rev. 43, 588–610. https://doi.org/10.1039/C3CS60235D.

Jakubek, M., Kejík, Z., Parchaňský, V., Kaplánek, R., Vasina, L., Martásek, P., Král, V., 2017. Water soluble chromone Schiff base derivatives as fluorescence receptor for aluminium(III). Supramol. Chem. 29, 1–7. https://doi.org/10.1080/10610278.2016.1153095.

Jamadar, A., Duhme-Klair, A.K., Vemuri, K., Sritharan, M., Dandawate, P., Padhye, S., 2012. Synthesis, characterisation and antitubercular activities of a series of pyruvate-containing aroyl-hydrazones and their Cu-complexes. Dalton Trans. 41, 9192–9201. https://doi.org/10.1039/c2dt30322a.

Jiang, C., He, Y., Liu, Y., 2020. Recent advances in sensors for electrochemical analysis of nitrate in food and environmental matrices. Analyst 145, 5400–5413. https://doi.org/10.1039/D0AN00823K.

Job, P., 1928. Formation and stability of inorganic complexes in solution. Ann. Chim. 9, 113–203.

Jun, M.E., Roy, B., Ahn, K.H., 2011. "Turn-on" fluorescent sensing with "reactive" probes. Chem. Commun. 47, 7583–7601. https://doi.org/10.1039/C1CC00014D.

Kajal, A., Bala, S., Kamboj, S., Sharma, N., Saini, V., 2013. Schiff bases: A versatile pharmacophore. J. Catal. 2013,. https://doi.org/10.1155/2013/893512 893512.

Karon, K., Lapkowski, M., 2015. Carbazole electrochemistry: a short review. J. Solid State Electr. 19, 2601–2610. https://doi.org/10.1007/s10008-015-2973-x.

Kaur, B.N., Kaur, B., 2017. Spectral studies on anthracene based dual sensor for Hg^{2+} and Al^{3+} ions with two distinct output modes of detection. Spectrochim. Acta A. 181, 60–64. https://doi.org/10.1016/j.saa.2017.03.029.

Kim, J.S., Noh, K.H., Lee, S.H., Kim, S.K., Kim, S.K., Yoon, J., 2003. Molecular Taekwondo. 2. A new calix[4]azacrown bearing two different binding sites as a new fluorescent ionophore. J. Org. Chem. 68, 597–600. https://doi.org/10.1021/jo020538i.

Kolcu, F., Erdener, D., Kaya, İ., 2021. Synthesis and characterization of a highly selective turn-on fluorescent chemosensor for Sn^{2+} derived from diimine Schiff base. Synth. Met. 272,. https://doi.org/10.1016/j.synthmet.2020.116668 116668.

Kolcu, F., Erdener, D., Kaya, İ., 2020. A Schiff base based on triphenylamine and thiophene moieties as a fluorescent sensor for Cr (III) ions: Synthesis, characterization and fluorescent applications. Inorg. Chim. Acta 509,. https://doi.org/10.1016/j.ica.2020.119676 119676.

Kolcu, F., Kaya, İ., 2016. Synthesis and characterization of novel conjugated polyphenols of terephthaldehyde derived from symmetrical bis-azomethine groups in the polymer backbone via oxidative polycondensation, Pure Appl. Chem. 53, 438-451.10.1080/10601325.2016.1176445.

Krewski, D., Yokel, R.A., Nieboer, E., Borchelt, D., Cohen, J., Harry, J., Kacew, S., Lindsay, J., Mahfouz, A.M., Rondeau, V., 2007. Human health risk assessment for aluminium, aluminium oxide, and aluminium hydroxide. J. Toxicol. Env. Heal. B 10, 1–269. https://doi.org/10.1080/10937400701597766.

Krupińska, I., 2020. Aluminium drinking water treatment residuals and their toxic impact on human health. Molecules 25, 641. https://doi.org/10.3390/molecules25030641.

Kumar, J., Sarma, M.J., Phukan, P., Kumar, D.D., 2015. A new simple Schiff base fluorescence "on" sensor for Al^{3+} and its living cell imaging. Dalton Trans. 44, 4576–4581. https://doi.org/10.1039/c4dt03932g.

Lakowicz, J.R., 1999. Principles of Fluorescence Spectroscopy. Kluwer Academic/Plenum Publishers, New York.

Li, Y.P., Zhao, Q., Yang, H.R., Liu, S.J., Liu, X.M., Zhang, Y.H., Hu, T.L., Chen, J.T., Chang, Z., Bu, X.H., 2013. A new ditopic radiometric receptor for detecting zinc and fluoride ions in living cells. Analyst 138, 5486–5494. https://doi.org/10.1039/C3AN00351E.

Likussar, W., Boltz, D., 1971. Theory of continuous variations plots and a new method for spectrophotometric determination of extraction and formation constants. Anal. Chem. 43, 1265–1272. https://doi.org/10.1021/ac60304a006.

Manna, A.K., Chowdhury, S., Patra, G.K., 2020. Combined experimental and theoretical studies on a phenyl thiadiazole-based novel turn-on fluorescent colorimetric Schiff base chemosensor for the selective and sensitive detection of Al^{3+}. New J. Chem. 44, 10819–10832. https://doi.org/10.1039/d0nj01954b.

Maya, S., Prakash, T., Das Madhu, K., Goli, D., 2016. Multifaceted effects of aluminium in neurodegenerative diseases: A review. Biomed. Pharmacother. 83, 746–754. https://doi.org/10.1016/j.biopha.2016.07.035.

Min, X., Yi, F., Han, X.L., Li, M., Gao, Q., Liang, X., Chen, Z., Sun, Y., Liu, Y., 2022. Targeted photodynamic therapy using a water-soluble aggregation-Induced emission photosensitizer activated by an acidic tumor microenvironment. Chem. Eng. J. 432,. https://doi.org/10.1016/j.cej.2021.134327 134327.

Na, N., Wang, F., Huang, J., Niu, C., Yang, C., Shang, Z., Han, F., Ouyang, J., 2014. An aggregation-induced emission-based fluorescent chemosensor of aluminium ions. RSC Adv. 4, 35459–35462. https://doi.org/10.1039/C4RA05095A.

Patil, D.Y., Patil, A.A., Khadke, N.B., Borhade, A.V., 2019. Highly selective and sensitive colorimetric probe for Al^{3+} and Fe^{3+} metal ions based on 2-aminoquinolin-3-yl-phenyl hydrazone Schiff base. Inorg. Chim. Acta 492, 167–176. https://doi.org/10.1016/j.ica.2019.04.006.

Perl, D.P., Brody, A.R., 1980. Alzheimer's disease: X-ray spectrometric evidence of aluminum accumulation in neurofibrillary tangle-bearing neurons. Science 208, 297–299. https://doi.org/10.1126/science.7367858.

Perlmutter, J.S., Tempel, L.W., Black, K.J., Parkinson, D., Todd, R.D., 1997. MPTP induces dystonia and parkinsonism, clues to the pathophysiology of dystonia. Neurology 49, 1432–1438. https://doi.org/10.1212/wnl.49.5.1432.

Polizzi, S., Pira, E., Ferrara, M., Bugiani, M., Papaleo, A., Albera, R., Palmi, S., 2002. Neurotoxic effects of aluminum among foundry workers and Alzheimer's disease. Neurotoxicology 23, 761–774. https://doi.org/10.1016/S0161-813X(02)00097-9.

Qu, S., Zheng, C., Liao, G., Fan, C., Liu, G., Pu, S., 2017. A fluorescent chemosensor for Sn^{2+} and Cu^{2+} based on a carbazole-containing diarylethene. RSC Adv. 7, 9833–9839. https://doi.org/10.1039/c6ra27339d.

Rahim, F., Ullah, H., Taha, M., Wadood, A., Javed, M.T., Rehman, W., Nawaz, M., Ashraf, M., Ali, M., Sajid, M., Ali, F., Khan, M. N., Khan, K.M., 2016. Synthesis and in vitro acetylcholinesterase and butyrylcholinesterase inhibitory potential of hydrazide based Schiff bases. Bioorg. Chem. 68, 30–40. https://doi.org/10.1016/j.bioorg.2016.07.005.

Rana, S., Mittal, S.K., Kaur, N., Banks, C.E., 2017. Disposable screen printed electrode modified with imine receptor having a wedge bridge for selective detection of Fe(II) in aqueous medium. Sensor Actuat. B-Chem 249, 467–477. https://doi.org/10.1016/j.snb.2017.04.135.

Roy, A., Nandi, M., Roy, P., 2021. Dual chemosensors for metal ions: A comprehensive review. Trends Anal. Chem. 138,. https://doi.org/10.1016/j.trac.2021.116204 116204.

Roy, P., 2021. Fluorescent chemosensors based on 4-methyl-2,6-diformylphenol. Coordin. Chem. Rev. 427,. https://doi.org/10.1016/j.ccr.2020.213562 213562.

Sahana, A., Banerjee, A., Lohar, S., Sarkar, B., Mukhopadhyay, S.K., Das, D., 2013. Rhodamine-based fluorescent probe for Al^{3+} through time-dependent PET-CHEF-FRET Processes and its cell staining application. Inorg. Chem. 52, 3627–3633. https://doi.org/10.1021/ic3019953.

Salarvand, Z., Amirnasr, M., Meghdadi, S., 2019. Colorimetric and fluorescent sensing of Al^{3+} by a new 2-hydroxynaphthalen based Schiff base "Off-On" chemosensor. J. Lumin. 207, 78–84. https://doi.org/10.1016/j.jlumin.2018.10.115.

Schiff, H., 1864. Mittheilungen aus dem universitats laboratorium in Pisa: Eine neue reihe organischer basen. Liebigs Ann. 131, 118–119. https://doi.org/10.1002/jlac.18641310113.

Seo, E.T., Nelson, R.F., Fritsh, J.M., Marcoux, L.S., Leedy, D.W., Adams, N., 1966. Anodic oxidation pathways of aromatic amines. Electrochemical and electron paramagnetic resonance studies. J. Am. Chem. Soc. 88, 3498–3503. https://doi.org/10.1021/ja00967a006.

Shah, S.S., Shah, D., Khan, I., Ahmad, S., Ali, U., Ur Rahman, A., 2020. Synthesis and antioxidant activities of Schiff bases and their complexes: An updated review. Biointerf. Res. Appl. Chem. 10, 6936–6963. https://doi.org/10.33263/BRIAC106.69366963.

Shyamal, M., Mazumdar, P., Maity, S., Sahoo, G.P., Morán, G.S., Misra, A., 2016a. Pyrene scaffold as real-time fluorescent turn-on chemosensor for selective detection of trace-level Al(III) and its aggregation-induced emission enhancement. J. Phys. Chem. A 120, 210–220. https://doi.org/10.1021/acs.jpca.5b09107.

Shyamal, M., Mazumdar, P., Maity, S., Samanta, S., Sahoo, G.P., Misra, A., 2016b. Highly selective turn-on fluorogenic chemosensor for Zn^{2+} based on chelation enhanced fluorescence. ACS Sens. 1, 739–747. https://doi.org/10.1021/acssensors.6b00289.

Singh, P., Singh, D.P., Tiwari, K., Mishra, M., Singh, A.K., Singh, V. P., 2015. Synthesis, structural investigations and corrosion inhibition studies on Mn(II), Co(II), Ni(II), Cu(II) and Zn(II) complexes with 2-amino-benzoic acid (phenyl-pyridin-2-yl-methylene)-hydrazide. RSC Adv. 5, 45217–45230. https://doi.org/10.1039/c4ra11929k.

Singh, V.P., Tiwari, K., Mishra, M., Srivastava, N., Saha, S., 2013. 5-[{(2-Hydroxynaphthalen-1-yl)methylene}amino]pyrmidine-2,4 (1H,3H)-dione as Al^{3+} selective colorimetric and fluorescent chemosensor. Sensor. Actuat. B-Chem. 182, 546–554. https://doi.org/10.1016/j.snb.2013.03.083.

Skalny, A.V., Aschner, M., Jiang, Y., Gluhcheva, Y.G., Tizabi, Y., Lobinski, R., Tinkov, A.A., 2021. Molecular mechanisms of aluminum neurotoxicity: Update on adverse effects and therapeutic strategies. Adv. Neurotoxicol. 5, 1–34. https://doi.org/10.1016/bs.ant.2020.12.001.

Soni, M.G., White, S.M., Flamm, W.G., Burdock, G.A., 2001. Safety evaluation of dietary aluminum. Regul. Toxicol. Pharmacol. 33, 66–79. https://doi.org/10.1006/rtph.2000.1441.

Tang, K.C., Chang, M.J., Lin, T.Y., Pan, H.A., Fang, T.C., Chen, K. Y., Hung, W.Y., Hus, Y.H., Chou, P.T., 2011. Fine tuning the energetics of excited-state intramolecular proton transfer (ESIPT): white light generation in a single ESIPT system. J. Am. Chem. Soc. 133, 17738–17745. https://doi.org/10.1021/ja2062693.

Teran, R., Guevara, R., Mora, J., Dobronski, L., Barreiro-Costa, O., Beske, T., Pérez-Barrera, J., Araya-Maturana, R., Rojas-Silva, P., Poveda, A., Herredia-Moya, J., 2019. Characterization of antimicrobial, antioxidant, and leishmanicidal activities of Schiff base derivatives of 4-aminoantipyrine. Molecules 24, 2696. https://doi.org/10.3390/molecules24152696.

Tiwari, K., Mishra, M., Singh, V.P., 2013. A highly sensitive and selective fluorescent sensor for Al^{3+} ions based on thiophene-2-carboxylic acid hydrazide Schiff base. RSC Adv. 3, 12124–12132. https://doi.org/10.1039/C3RA41573B.

Udhayakumari, D., Inbaraj, V., 2020. A review on Schiff base fluorescent chemosensors for cell imaging applications. J. Fluores. 30, 1203–1223. https://doi.org/10.1007/s10895-020-02570-7.

Walton, J.R., 2006. Aluminum in hippocampal neurons from humans with Alzheimer's disease. Neurotoxicology 27, 385–394. https://doi.org/10.1016/j.neuro.2005.11.007.

Wang, G.Q., Qin, J.C., Li, C.R., Yang, Z.Y., 2015. A highly selective fluorescent probe for Al^{3+} based on quinoline derivative. Spectrochim. Acta A 150, 21–25. https://doi.org/10.1016/j.saa.2015.05.041.

Weller, D.G., Gutierrez, A.J., Rubio, C., Revert, C., Hardisson, A., 2010. Dietary intake of aluminum in a Spanish population (Canary islands). J. Agr. Food Chem. 58, 10452–10457. https://doi.org/10.1021/jf102779t.

Wilmott, J.M., Aust, D.T., Crawford, T.K., 2004. inventors; Lab21 Inc, assignee. Method for producing customized cosmetic and pharmaceutical formulations on demand. United States patent US 6,782,307.

Wu, D., Sedgwick, A.C., Gunnlaugsson, T., Akkaya, E.U., Yoon, J., James, T.D., Fluorescent chemosensors: the past, present and future. 2017. Chem. Soc. Rev. 46, 7105-7123. 10.1039/C7CS00240H.

Wu, J.S., Liu, W.M., Zhuang, X.Q., Wang, F., Wang, P.F., Tao, S.L., Zhang, X.H., Wu, S.K., Lee, S.T., 2007. Fluorescence turn on of coumarin derivatives by metal cations: A new Signaling mechanism based on C=N isomerization. Org. Lett. 9, 33–36. https://doi.org/10.1021/ol062518z.

Yadav, S., Yousuf, I., Usman, M., Ahmad, M., Arjmand, F., Tabassum, S., 2015. Synthesis and spectroscopic characterization of diorganotin(iv) complexes of N′-(4-hydroxypent-3-en-2-ylidene) isonicotinohydrazide: chemotherapeutic potential validation by in vitro interaction studies with DNA/HSA, DFT, molecular docking and cytotoxic activity. RSC Adv. 5, 50673–50690. https://doi.org/10.1039/C5RA06953J.

Yan, J., Fan, L., Qin, J.C., Li, C.R., Yang, Z.Y., 2016. A novel chromone Schiff-base fluorescent chemosensor for Cd(II) based on C=N Isomerization. J. Fluores. 26, 1059–1065. https://doi.org/10.1007/s10895-016-1794-3.

Yang, L.L., Zhu, W.J., Fang, M., Wu, Z.Y., Zhang, Q., Li, C., 2013. A new carbazole-based Schiff-base as fluorescent chemosensor for selective detection of Fe^{3+} and Cu^{2+}. Spectrochim. Acta A 109, 186–192. https://doi.org/10.1016/j.saa.2013.02.043.

Yin, Y., Chen, Z., Li, R.H., Yuan, C., Shao, T.Y., Wang, K., Tan, H., Sun, Y., 2021. Ligand-triggered platinum(ii) metallacycle with mechanochromic and vapochromic responses. Inorg. Chem. 60, 9387–9393. https://doi.org/10.1021/acs.inorgchem.1c00233.

Yoon, K.R., Ko, S.O., Lee, S.M., Lee, H., 2007. Synthesis and characterization of carbazole derived nonlinear optical dyes. Dyes Pigments 75, 567–573. https://doi.org/10.1016/j.dyepig.2006.07.

Yu, M.H., Hu, T.L., Bu, X.H., 2017. A metal–organic framework as a "turn on" fluorescent sensor for aluminum ions. Inorg. Chem. Front. 4, 256–260. https://doi.org/10.1039/c6qi00362a.

Yu, S.Y., Wu, S.P., 2014. A highly selective turn-on fluorescence chemosensor for Hg(II) and its application in living cell imaging. Sensor Actuat. B-Chem. 201, 25–30. https://doi.org/10.1016/j.snb.2014.04.077.

Zhu, H., Fan, J., Wang, B., Peng, X., 2015a. Fluorescent, MRI, and colorimetric chemical sensors for the first-row d-block metal ions.

Chem. Soc. Rev. 44, 4337–4366. https://doi.org/10.1039/C4CS00285G.

Zhu, J., Zhang, Y., Wang, L., Sun, T., Wang, M., Wang, Y., Ma, D., Yang, Q., Tang, Y., 2016. A simple turn-on Schiff base fluorescence sensor for aluminum ion. Tetrahedron Lett. 57, 3535–3539. https://doi.org/10.1016/j.tetlet.2016.06.112.

Zhu, W., Yang, L., Fang, M., Wu, Z., Zhang, Q., Yin, F., Huang, Q., Li, C., 2015b. New carbazole-based Schiff base: Colorimetric chemosensor for Fe^{3+} and fluorescent turn-on chemosensor for Fe^{3+} and Cr^{3+}. J. Lumin. 158, 38–43. https://doi.org/10.1016/j.jlumin.2014.09.020.

Zhu, W.J., Wu, Z.Y., Song, J.M., Li, C., 2011. Preparation and properties of two new soluble carbazole-containing functional polyacetylenes. Chin. Chem. Lett. 22, 1017–1020. https://doi.org/10.1016/j.cclet.2011.05.008.